Graphene-enabled terahertz dielectric rod antenna with polarization reconfiguration

Saeed Fakhte[1] · Mohammad Mahdi Taskhiri[1]

Abstract

In this article, magnetically biased graphene is utilized to achieve a terahertz antenna capable of reconfiguring the polarization of the radiation pattern, transitioning between two states of linear and circular polarizations. The antenna is structured in a way that allows terahertz waves to enter through a slot aperture from a microstrip transmission line. These waves are then coupled to a silicon dielectric resonator, which has a graphene layer on top of it. Subsequently, the terahertz surface waves are launched within the silicon dielectric rod by the dielectric resonator. By applying a biased magnetic field perpendicular to the antenna, the conductivity tensor of graphene exhibits non-diagonal elements. This results in the production of circular polarization within the antenna. Furthermore, altering the direction of the applied bias magnetic field causes a shift in polarization from right-hand circularly polarized to left-hand circularly polarized. The modified relaxation-effect model is employed at terahertz frequencies to calculate the losses of silver metal, deviating from the accurate skin effect model used for microwave frequencies. Remarkable impedance matching is attained for linear and circular polarization within the range of 2.86 to 3.14 THz. The article provides detailed insights into the simulated reflection coefficient, axial ratio, gain, and radiation patterns. This device holds the potential for integration into diverse subwavelength terahertz systems.

Keywords Terahertz (THz) antenna · Non-reciprocal graphene · Dielectric rod antenna (DRA)

1 Introduction

The terahertz frequency band, ranging from 0.1 to 10 THz, has gained attention for its unique properties and potential applications. Terahertz waves can penetrate various materials, making them suitable for non-destructive testing and spectroscopic analysis. They offer high bandwidths for wireless communication and find use in security screening, medical imaging, quality control, and material research. However, realizing the full potential of the terahertz frequency band requires technological advancements and overcoming signal

✉ Saeed Fakhte
fakhte@qut.ac.ir

1 Department of Electrical and Computer Engineering, Qom University of Technology, Qom, Iran

propagation and generation challenges (Pawar et al. 2013; Song and Nagatsuma 2011; Petrov et al. 2016; Elayan et al. 2018).

Terahertz antennas are essential for terahertz communication systems operating from 0.1 to 10 THz. They enable high-speed wireless communication, imaging, and sensing. However, designing efficient terahertz antennas is challenging due to the unique characteristics of this frequency range. The small wavelength size, ranging from 30 to 3000 μm, makes it challenging to fabricate antennas with matching dimensions. Advanced fabrication techniques and precise materials are required to overcome this challenge (He 2020; Fakhte and Taskhiri 2022; Singhwal et al. 2022).

Circularly polarized terahertz antennas are designed to radiate electromagnetic waves with circular polarization. Circular polarization offers advantages over linear polarization in robustness against signal fading caused by multipath propagation and improved signal quality. Circularly polarized terahertz antennas find applications in satellite communication, radar systems, and wireless sensor networks. Circular polarization provides better link stability compared to linear polarization. It reduces the impact of polarization mismatch between the transmitting and receiving antennas, ensuring a more reliable and consistent connection. Circular polarization helps to minimize the effects of multipath interference, which can degrade signal quality. This is particularly important in terahertz communication systems where line-of-sight propagation is limited, and signals are prone to scattering and reflection. Circular polarization is independent of the antenna's orientation or the direction of propagation, making it suitable for applications where antenna alignment may vary or change over time (Khan et al. 2023; Varshney et al. 2020; Aqlan et al. 2021; Wu and Zeng 2019).

Terahertz antenna design faces the challenge of achieving reconfiguration between polarizations. Reconfigurable antennas enable dynamic switching between linear and circular polarization states, enhancing the flexibility and adaptability of terahertz communication systems (Luo et al. 2019; Rasilainen et al. 2023; Venkatesh et al. 2022). To address this, researchers are exploring metamaterials, plasmonics, and MEMS techniques. Metamaterial-based antennas utilize engineered structures with unique electromagnetic properties, while plasmonic-based antennas exploit surface plasmon resonance. MEMS-based antennas incorporate micro-scale components for reconfiguration (Liu et al. 2022; Ali et al. 2022; Yang et al. 2022). In summary, efficient terahertz antenna design is complex due to the unique characteristics of terahertz waves. Circularly polarized and reconfigurable antennas offer promising solutions for addressing communication system challenges. Continued research in these areas will advance terahertz technologies with enhanced performance and functionality.

Dielectric rod antennas offer numerous advantages in the terahertz region. They provide high gain and directivity, which allows for a more focused beam of radiated energy. This is particularly valuable in applications that require precise targeting and high resolution, such as imaging and sensing systems (Ahmadi et al. 2023; Ali et al. 2022a, 2022b). Additionally, dielectric materials used in these antennas have low losses at terahertz frequencies, resulting in efficient transmission and reception. Dielectric rod antennas also offer design flexibility, as the dimensions of the rod can be adjusted to optimize performance (Sugimoto et al. 2022; Dukhopelnykov et al. 2020; "Rivera-Lavado et al. 2019). Furthermore, these antennas can support multiple polarization states, making them suitable for applications that require specific polarization for optimal functionality. Overall, dielectric rod antennas are well-suited for terahertz applications such as wireless communication, imaging, and sensing, where efficient and precise radiation is crucial. These advantages make dielectric rod antennas well-suited for terahertz applications such as wireless communication,

imaging, and sensing, where efficient and accurate radiation is essential (Nasir et al. 2019, 2022; Huang et al. 2019).

Graphene, an atom-thin carbon material arranged in a hexagonal lattice, garners interest in terahertz technology. Its exceptional properties, including excellent electrical conductivity, high carrier mobility, and broad absorption, make it promising for circularly polarized and reconfigurable terahertz antennas. By incorporating graphene into simple antenna designs like dipole or patch antennas, circularly polarized radiation can be easily produced. The unique characteristics of graphene, such as its controllable electrical conductivity with an applied voltage, enable reconfigurable antennas to adapt to changing channel conditions, interference, or user preferences. The electrical conductivity alteration influences the antenna's resonant frequency, providing tunability. Consequently, reconfigurable antennas can operate in multiple frequency bands, accommodating various communication standards and wireless applications. Additionally, graphene's high carrier mobility ensures swift response times and low power consumption, making it an optimal material for reconfigurable terahertz antennas. The ability to dynamically reconfigure these antennas allows for beam steering, spatial filtering, and beamforming, enhancing signal quality and reception in THz communication systems.

The following review examines various examples of reported work on terahertz antennas that involve polarization reconfiguration. A hybrid dual-frequency polarized reconfigurable THz antenna was designed and studied in Zhang et al. (2021a). The use of graphene meta-surface and TOPAS allowed for tunable polarization conversion and circular polarization. The polarization state of the two bands could be changed without reconstructing the structure by electrically shifting the Fermi energy of both graphene layers. Incorporating a monopole antenna with a graphene-based dual-band active polarization converter meta-surface (APCM) proposed a dual-band polarization reconfigurable terahertz antenna (Lv et al. 2020). The APCM unit cell had two perpendicular slots on the top and two biased graphene patches on the bottom. The chemical potentials of graphene could be adjusted from 0 to 0.5 eV to switch the APCM from ON (polarization conversion) to OFF in dual-band. In Kiani et al. (2023a), the study presented the design of a circular patch antenna with a cross-shaped slot using graphene. The antenna could reconfigure its frequency and was designed for a central frequency of 1.6 THz. Placing the cross-shaped slot in the center of the circular patch resulted in two orthogonal physical arms, enabling circular polarization. The antenna exhibited favorable characteristics in terms of matching and polarization within the frequency range of 0.5 THz to 2 THz, with a S11 parameter below -15 dB and an axial ratio below 2 dB. In Kiani et al. (2023b), a reconfigurable microstrip patch antenna was designed using a combination of graphene and gold. The antenna could access different types of right-hand circular polarization (RHCP) and left-hand circular polarization (LHCP) by simply switching the positions of its slots. The primary approach of the study was based on the principle that by rotating the position of the slot by 90°, the polarization could be switched from RHCP to LHCP. Furthermore, the researchers utilized the capacity of graphene to achieve frequency reconfigurability. In Moradi and Karimi (2023), the research paper presented a patch antenna designed for terahertz frequencies with a unique shape and feeding mechanism. The patch was capable of changing between three different shapes (triangle, rectangle, circle) and also had a slot, all achieved through the use of graphene. This allowed the antenna to simultaneously utilize the advantages of different patch shapes within a single structure. The resonance frequency of the antenna could be adjusted in the range of 3.8 to 5.3 THz, and the polarization could be changed between linear and circular polarization, resulting in a reconfigurable antenna for both frequency and polarization. In summary, all the reported works incorporate structures with small graphene layers in the

antenna structure. Nevertheless, the radiation patterns obtained in different polarizations do not exhibit complete symmetry due to the loading of these layers.

This paper proposes a dielectric rod antenna that incorporates graphene to enable the switching of polarization types and senses. The polarization and frequency band of operation can be reconfigured using the chemical potential of graphene and an external magnetic bias. Unlike previous studies that solely relied on the chemical potential parameter of graphene for polarization reconfiguration, this research also introduces the magnetic bias field as an additional parameter. While previous studies focused on altering graphene's chemical potential, this work achieves circular polarization by implementing a magnetic bias on graphene, which creates an anisotropic conductivity tensor within the material. In terms of innovation, this article introduces a dielectric rod antenna with the capability to reconfigure between linear and circular polarization. A thorough examination of the existing literature reveals the absence of previous reports on a dielectric rod antenna with this distinctive capability, not only in the terahertz band but also across other frequency bands. This achievement has been accomplished by incorporating anisotropic graphene into the antenna structure, which is a unique approach that has not been previously reported in dielectric rod antennas.

2 Antenna configuration

The proposed cylindrical dielectric rod antenna incorporating a graphene sheet is illustrated in Fig. 1. The dielectric rod, constructed from SiO_2 material with a relative permittivity of 3.8, possesses a diameter (d_{Rod}) and height (h_{Rod}). A dielectric rod is placed on a dielectric resonator loaded with graphene. The diameter and height of the cylindrical dielectric resonator are d and h_{Si}, respectively. The dielectric resonator is made of silica (Si). The circular graphene sheet has a diameter (d_g), and its thickness is assumed to be 1 nm. Graphene is often placed on a SiO_2 (silicon dioxide) layer because of its unique properties and compatibility with silicon-based electronics. The thickness of the SiO_2 layer is h_{SiO2}. The dielectric resonator is also placed on a slot with the dimensions of $l_s \times w_s$. Terahertz waves are coupled to the antenna from the microstrip transmission line placed at the bottom of the SiO_2 layer by using the slot aperture on the ground plane of the antenna. To apply the magnetostatic field, a solenoid can be placed beneath the antenna, as shown in Fig. 1b. It is clear that the magnetostatic field applied from the solenoid to the antenna is primarily vertical with a z component. Adjusting the current through the solenoid allows for easy control of the strength of the magnetostatic field. This arrangement enables the examination of graphene's anisotropic properties under varying magnetic field intensities.

The surface impedance model is a helpful tool for simplifying the modeling of metals at low terahertz frequencies. It considers relaxation effects and is employed to calculate the surface impedance between 0.1 and 10 THz due to the significant wave penetration into the metal and electron–phonon collisions (Lucyszyn 2007). While the skin effect model is commonly used in microwave frequencies, it is not as accurate in terahertz frequencies. Therefore, in the simulation of this antenna, its surface impedance model has been used instead of silver metal.

$$Z_S(\omega) = \sqrt{\frac{j\omega\mu_0\mu_r}{\sigma_R + j\omega\varepsilon_0}}, \quad \sigma_R = \frac{\sigma_o}{(1 + j\omega\tau)} \tag{1}$$

Silver metal exhibits the following parameter values at low THz frequencies: the direct current intrinsic bulk conductivity is designated as $\sigma_0 = 6.1 \times 10^7 S/m$, the metal's

Fig. 1 The geometry of the proposed antenna, **a** The configuration of a dielectric rod antenna integrated with magnetically-biased graphene. The design incorporates a direct current (DC) magnetic bias, denoted as B_0, which is oriented along the Z-axis, **b** Proposed magnetic flux density application method utilizing a solenoid positioned beneath the antenna

(a)

(b)
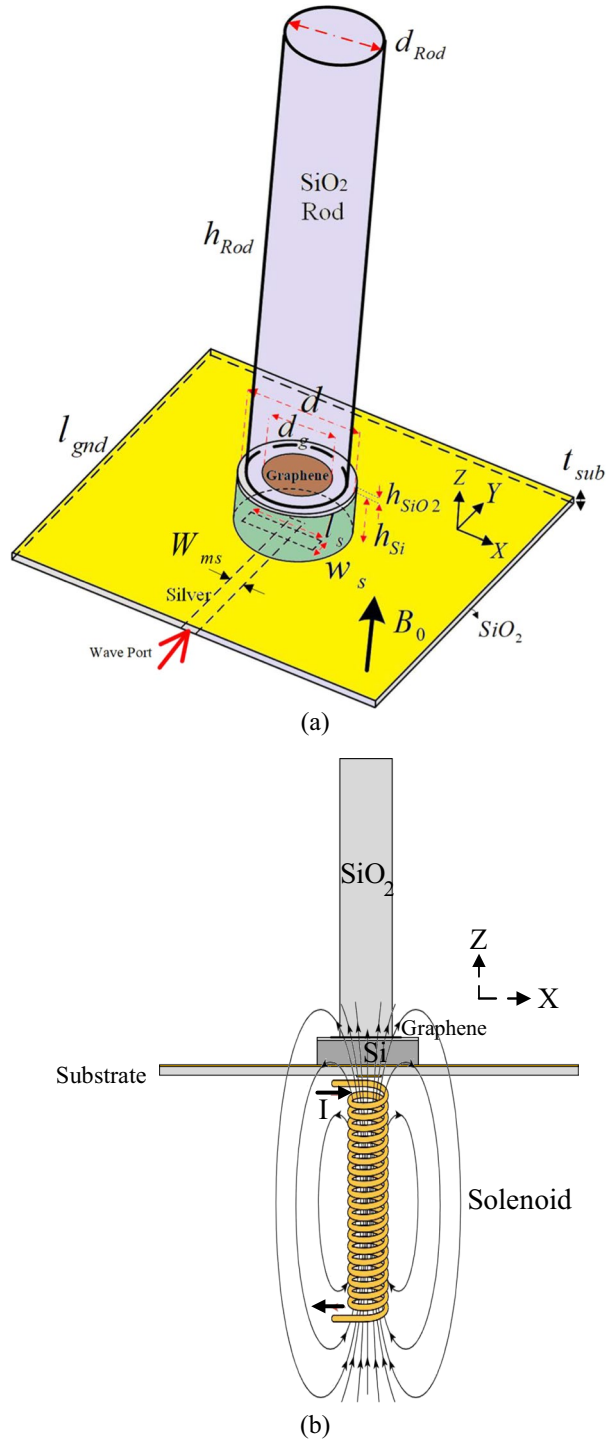
permeability coefficient is expressed as $\mu_r = 0.99998$, and the phenomenological scattering relaxation time for the free electrons is $\tau = 38.182 \times 10^{-14} s$. The angular frequency is denoted as ω, while the permittivity of free space is represented by ε_0 and the permeability of free space by μ_0. The intrinsic bulk conductivity of the metal is symbolized as σ_R.

3 Design considerations

In this section, we will discuss the design of a rod antenna fed with a slot and a graphene-loaded dielectric resonator. It is important to note that the antenna's functional band is determined by the resonant modes of the slot and the dielectric resonator (DR). Therefore, it is necessary to provide formulas to calculate the resonance frequency of the graphene-loaded DR modes. To simplify the process and obtain a preliminary estimate, we can use the formula for the resonance frequency of the HEM_{111} mode of graphene-loaded cylindrical dielectric resonator mode. For this purpose, the following equations, which have been proven by the authors in another work, are used (Fakhte and Taskhiri 2023):

$$\begin{cases} k_z h_{Si} = \pi + \tan^{-1}\left(\dfrac{4\pi f_r \varepsilon_r \varepsilon_0 k_z X_g}{(2\pi f_r)^2 (\varepsilon_r \varepsilon_0)^2 X_g^2 - k_z^2} \right) \\ \left(\dfrac{3.682}{d} \right)^2 + k_z^2 = (2\pi f_r)^2 \varepsilon_r \varepsilon_0 \mu_0 \end{cases} \tag{2}$$

$$\begin{cases} k_z h_{Si} = \pi + \tan^{-1}\left(\dfrac{4\pi f_r \varepsilon_r \varepsilon_0 k_z X_g}{(2\pi f_r)^2 (\varepsilon_r \varepsilon_0)^2 X_g^2 - k_z^2} \right) \\ \left(\dfrac{3.682}{d} \right)^2 + k_z^2 = (2\pi f_r)^2 \varepsilon_r \varepsilon_0 \mu_0 \end{cases} \tag{3}$$

where c is the speed of light in free space, d is the diameter of the silicon dielectric resonator, X_g is the imaginary part of the graphene surface impedance, H_{Si} is the height of the dielectric resonator, and ε_r is the permittivity of the dielectric resonator. By solving Eqs. (2) and (3) simultaneously, we can obtain the values of two unknowns, f_r, and k_z. Using the Kubo formula, the conductivity of graphene can be obtained as follows (Shiau 1976):

$$\sigma_g(\omega) = \frac{e^2 k_B T \tau}{(1 + j\omega\tau)\pi\hbar^2} \left[\frac{\mu_c}{k_B T} + 2\ln\left(e^{-\mu_c/k_B T} + 1 \right) \right] \tag{4}$$

This formula involves various parameters, including the reduced Plank constant (ℏ), angular frequency (ω), Boltzmann constant (k_B), relaxation time (τ), and temperature (T). For this particular study, a temperature of 300 K, a chemical potential of 0.23 eV, and a relaxation time of 0.9 ps are considered. To modify the chemical potential of graphene (μ_c), an electrostatic voltage source is utilized. The impedance of graphene is then determined using the following method:

$$Z_g(\omega) = \frac{1}{\sigma_g(\omega)} \tag{5}$$

Therefore, the value of the imaginary part of the impedance at the design frequency of 3 terahertz is equal to 800 ohms. By substituting $Xg = 800\Omega$ and $\varepsilon_r = 11.9$ into Eqs. (2) and (3), we can determine that the dimensions of DR at a frequency of 3 terahertz are $d = 34$um and $hsi = 6.9$um. The resonance frequency in the biased state with a DC magnetic field of B_0

closely approximates the dimensions obtained for unbiased graphene. To validate the structure's performance, simulations were conducted using HFSS software. It is essential to mention that the relaxation effect model for silver metal was employed in these simulations.

The rod's diameter is determined by choosing a value within the range of d_{min} and d_{max} (Gusynin et al. 2006).

$$d_{max} \approx \frac{\lambda_0}{\sqrt{\pi(\varepsilon_r - 1)}} \tag{6}$$

$$d_{min} \approx \frac{\lambda_0}{\sqrt{2.5\pi(\varepsilon_r - 1)}} \tag{7}$$

where λ_0 represents the wavelength in free space that corresponds to the band's middle frequency. Consequently, considering a 3 THz central frequency, it is advisable to select a rod diameter ranging from 21.3 to 33.7 µm. Furthermore, the recommended initial length for the rod is set at 700 µm. To further enhance the antenna's performance, the next step involves utilizing HFSS software to optimize its gain, reflection coefficient, and impedance bandwidth. The optimized values for all parameters are listed in Table 1.

To achieve circular polarization, it is necessary to generate two electric field components with the same amplitude and a phase difference of 90° in the radiation pattern. This is accomplished by utilizing the anisotropic tensor of graphene conductivity. In our simulation analyses, we utilize the Kubo model in conjunction with a surface conductivity tensor (Sounas and Caloz 2012) to establish a graphene layer that encounters a perpendicular magneto-static field.

$$\overline{\sigma} = \begin{bmatrix} \sigma_{xx} & -\sigma_{yx} & 0 \\ \sigma_{yx} & \sigma_{yy} & 0 \\ 0 & 0 & 0 \end{bmatrix} \tag{8}$$

The elements of the tensor, denoted as σ_{xx} and $\sigma_{yx} = -\sigma_{xy}$, represent the diagonal and off-diagonal components, respectively.

$$\sigma_{xx}(\omega, B_0) = \sigma_0 \frac{1 + j\omega\tau}{(\omega_c\tau)^2 + (1 + j\omega\tau)^2} \tag{9}$$

$$\sigma_{yx}(\omega, B_0) = \sigma_0 \frac{\omega_c\tau}{(\omega_c\tau)^2 + (1 + j\omega\tau)^2}$$

$$\sigma_0 = \frac{2e^2\tau}{\pi\hbar^2} k_B T \ln\left(2\cosh\frac{\mu_c}{2k_B T}\right), \quad \omega_c = eB_0 v_F^2/\mu_c \tag{10}$$

Table 1 The optimized dimensions of the proposed antenna. Unit: µm

Parameter	d	h_{si}	h_{SiO2}	d_g	d_{Rod}	h_{Rod}	l_s	w_s	l_{gnd}	W_{ms}	t_{sub}
value	34	6.9	0.25	28	26	1000	16.5	2	120	3.5	1.6

where $\mu_c, e, k_B, \tau, T, \hbar, \omega, v_F, \omega_c$, and B_0 are chemical potential, electron charge, Boltzmann's constant, carrier relaxation time, temperature, reduced Plank's constant, Fermi velocity, angular frequency, cyclotron frequency, and magnetic flux density, respectively. Equations (9) and (10) are utilized with a chemical potential of 0.23eV, a temperature of 300K, a DC magnetic flux density $B_0 = 4.6T$, and a relaxation time of 0.9 ps. The resulting diagonal and off-diagonal elements of the tensor are plotted in Fig. 2. These values were chosen to achieve optimal reconfigurability between linear and circular polarization. Notably, the figure demonstrates that the frequency of 3 TH exhibits the most significant disparity between σ_{xx} and σ_{yx}, indicating the potential for circular polarization in the antenna.

To calculate the magnetostatic field of a solenoid, the following formula can be applied (Johnk 1975):

$$B = \mu \frac{NI}{L} \tag{11}$$

where μ represents the permeability of the core, N denotes the number of wires turns, I represents the current passing through the solenoid, and L denotes the length of the solenoid. By utilizing a ferrite material with a permeability (μ) value of 2000 for the core of the solenoid, along with selecting the solenoid's parameters as follows: N=7 (number of
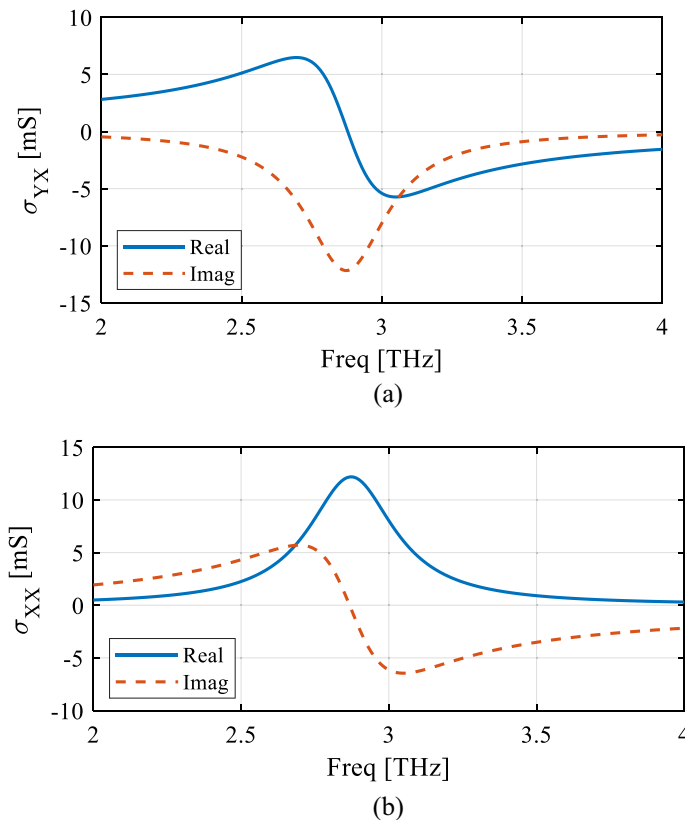

Fig. 2 The tensor's diagonal and off-diagonal elements of graphene surface conductivity, denoted as **a** σ_{yx} and **b** σ_{xx}, are analyzed for $\mu_c = 0.23eV, T = 300K, \tau = 0.9ps, B_0 = 4.6T$

turns), L = 3.82 mm (length), and I = 1A (current), it is possible to generate a powerful magnetic field of 4.6 T along the axis of the solenoid. One specific example of a ferrite material with a permeability of 2000 is TDK's Mn-Zn ferrite (Corporation 2023).

While it is true that utilizing a static magnetic field source can introduce complexity to the structure, the numerous intriguing features it brings to devices have led to the widespread exploration of magnetically biased graphene in various studies. Despite the additional challenges, researchers have reported its potential and showcased its capabilities in numerous works (Larki et al. 2019; Dolatabady and Granpayeh 2019; Tamagnone et al. 2018).

To estimate the power consumption, it is assumed that the diameter of the copper wire used in the solenoid is 0.2 mm, and the diameter of the solenoid ring is 0.6 mm. Based on these assumptions, the DC resistance of the entire solenoid wire is approximately 4.9 mΩ. Considering a current of 1 A flowing through the solenoid, the power consumption is approximately 4.9 mW.

4 Results and discussion

The results of the proposed antenna's simulation for linear and circular polarization states were achieved by varying the magnetic bias value. In Fig. 3, one can observe graphs displaying the reflection coefficient, axial ratio, and gain for two distinct DC magnetic bias values. These graphs reveal that adjusting the B_0 value from 0 to −4.6T causes a shift in the antenna's polarization from linear to right-hand circular. The antenna exhibits an impedance bandwidth of 2.9–3.98 THz in linear polarization mode, as demonstrated in Fig. 3a. However, when a DC magnetic bias is applied, this bandwidth expands to 2.84–3.86 THz.

Terahertz spectroscopy, utilizing the 3THz frequency, can differentiate between different hydrate forms. Lactose, a commonly used excipient in the pharmaceutical industry, has three distinct hydrate forms: a-monohydrate, a-anhydrate, and b-anhydrate. These forms exhibit terahertz spectra suitable for quantitative and qualitative analysis. The terahertz region's unique sensitivity to lattice structure enables the study of both crystalline and amorphous materials qualitatively and quantitatively (Pawar et al. 2013; Song and Nagatsuma 2011; Petrov et al. 2016).

Figure 3b displays the effect of changing B_0 on the antenna's linear gain. The maximum gain value of 17.5 dB transforms into a left-hand circular gain with a maximum value of 16.4 dB. The reduction in circular polarization mode's gain is attributed to increased losses caused by the rise in σ_{xx} and σ_{yx} resulting from applying B_0. Furthermore, Fig. 3c depicts that applying B_0 diminishes the axial ratio from above 50 dB to below 3 dB, indicating the antenna's favorable performance in circular polarization.

The shift from +z to −z direction in the applied DC magnetic bias in Fig. 1 alters the circular polarization mode of the antenna. It transforms the left-hand circular polarization mode into a right-hand circular polarization mode. Surprisingly, despite this change, the reflection coefficient, gain, and axial ratio diagrams remain constant, as shown in Fig. 4. This consistent behavior demonstrates the high efficiency of the presented technique. Moreover, the method's effectiveness can be attributed to the symmetrical nature of the structure. Compared to other reconfiguration methods that require structural manipulation, such as insertion or cutting, this approach ensures no discrepancies between left-handed (LH) and right-handed (RH) outcomes.
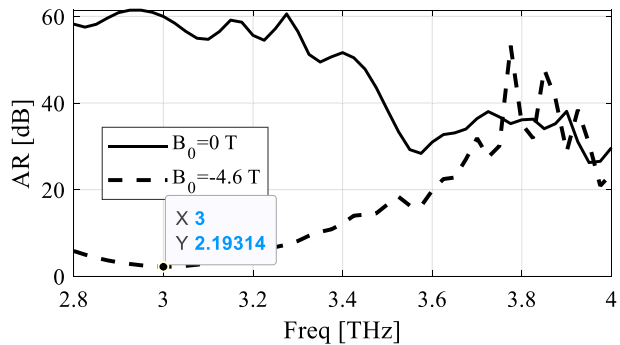
Fig. 3 The simulated results of the polarization reconfigurable dielectric rod antenna for two values of magnetic flux density, $B_0 = 0, -4.6T$ (a) reflection coefficients, **b** gains, and **c** axial ratios. Other parameters of graphene are $\mu_c = 0.23eV, T = 300K, \tau = 0.9ps$
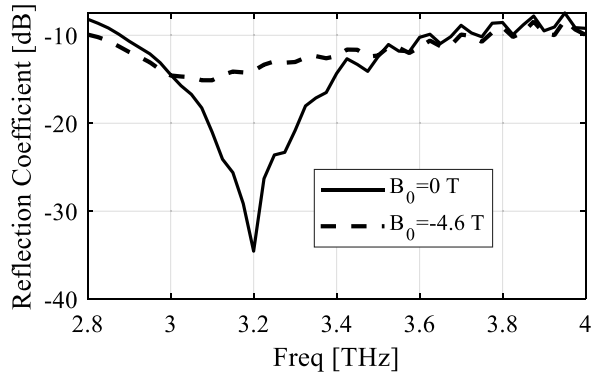

(a)
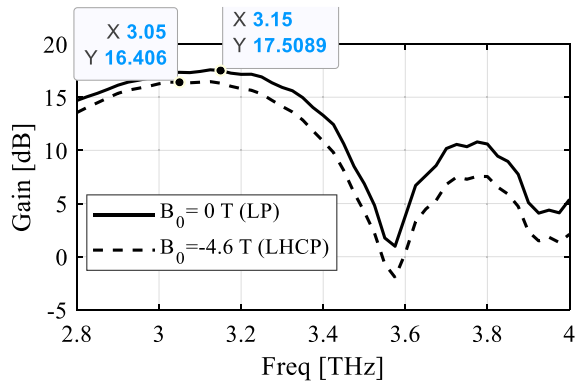
(b)

(c)

The distribution of the electric field inside the dielectric rod antenna at a frequency of 3 THz is shown in Fig. 5. As can be seen in the figure, by applying DC magnetic bias equal to − 4.6 T, rotation in the electric field along the rod has been achieved.

In Fig. 6, the radiation patterns of the antenna are displayed. Various DC magnetic bias values were examined. When the magnetic bias is oriented along the z-axis, with a magnitude of $B_0 = -4.6Ta_z$ (Fig. 6a, b), the pattern demonstrates a predominance of left-handed

Fig. 4 The simulated results of the polarization reconfigurable dielectric rod antenna for two directions of magnetic flux density, $B_0 = +4.6a_zT, -4.6a_zT$ **a** reflection coefficients, **b** axial ratios, and **c** gains. Other parameters of graphene are $\mu_c = 0.23eV, T = 300K, \tau = 0.9ps$

(a)

(b)

(c)
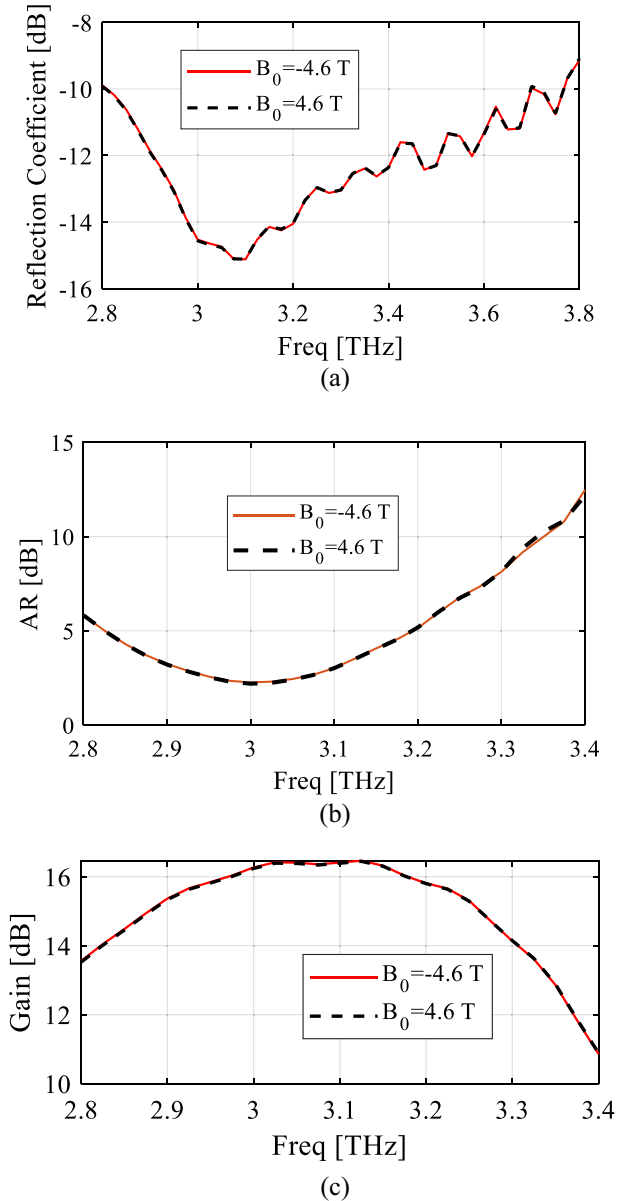
circular polarization. Conversely, in Fig. 6c, d, when the magnetic bias is directed in the opposite direction, the pattern exhibits predominantly right-handed circular polarization. When the DC magnetic bias is deactivated, the pattern primarily shows linear polarization, as shown in Fig. 6f, e. Also, in this figure, it can be observed that simulated patterns generated by COMSOL and HFSS software are in good agreement across all three polarizations. More specifically, the circular polarization shows excellent cross-polar discrimination between the RHCP and LHCP components of the pattern. Furthermore, in the linear polarization, the cross
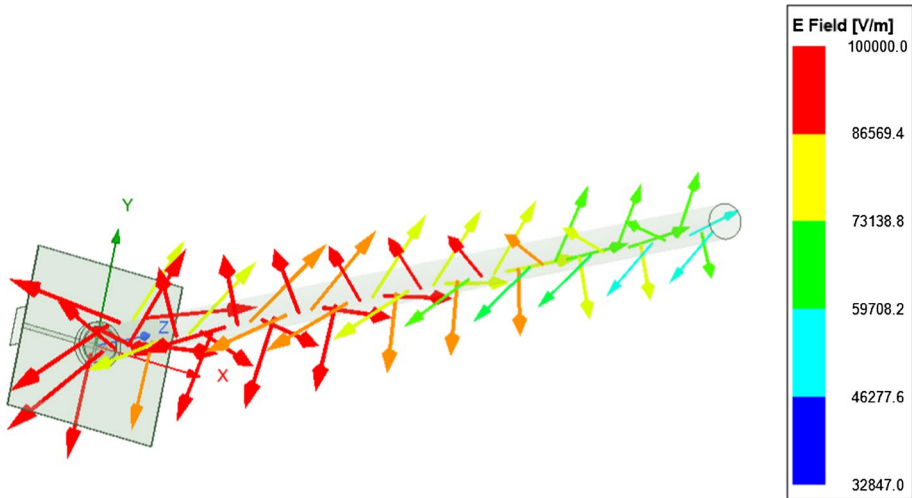
Fig. 5 The electric field distribution of the dielectric rod antenna at 3 THz for $B0 = -4.6a_z$. $\mu_c = 0.23eV, T = 300K, \tau = 0.9ps$

components are at least 17 dB lower than the dominant component. Furthermore, broadside patterns have been obtained in both XoZ and YoZ pages.

To ensure the precision and dependability of the simulation findings acquired through the HFSS software, we have used COMSOL, a different software, for validation purposes. We aim to conduct a comprehensive analysis and comparison of the simulation outcomes from both software programs, with the ultimate objective of establishing the consistency and credibility of the results.

Figure 7 showcases a detailed comparative examination of the simulation outcomes derived from both HFSS and COMSOL software. It is worth noting that the figure presents a remarkable correlation concerning the reflection coefficient, gain, and radiation patterns. These findings serve as robust evidence, further substantiating the validity of the simulation results.

In Table 2, a comparison is shown between the newly developed terahertz antenna, which offers polarization reconfiguration capability, and antennas discussed in prior research papers (Zhang et al. 2021b; Kiani et al. 2020, 2021a, b, c, 2022, 2023c; Chashmi et al. 2019, 2020a, 2020b). The comparison reveals that the proposed antenna outperforms the reported antennas in terms of radiation efficiency for both linear and circular polarization operations. Additionally, unlike the proposed antenna, none of the antennas mentioned in Zhang et al. 2021b; Kiani et al. 2020, 2021a, b, c, 2022, 2023c; Chashmi et al. 2019; Chashmi et al. 2020a; Chashmi et al. 2020b) exhibit identical LHCP and RHCP radiation patterns. Another important highlight is the introduction of a novel approach in this study, which utilizes magnetically biased graphene to achieve circular polarization. This contrasts previous references that employed non-biased graphene for the same purpose.
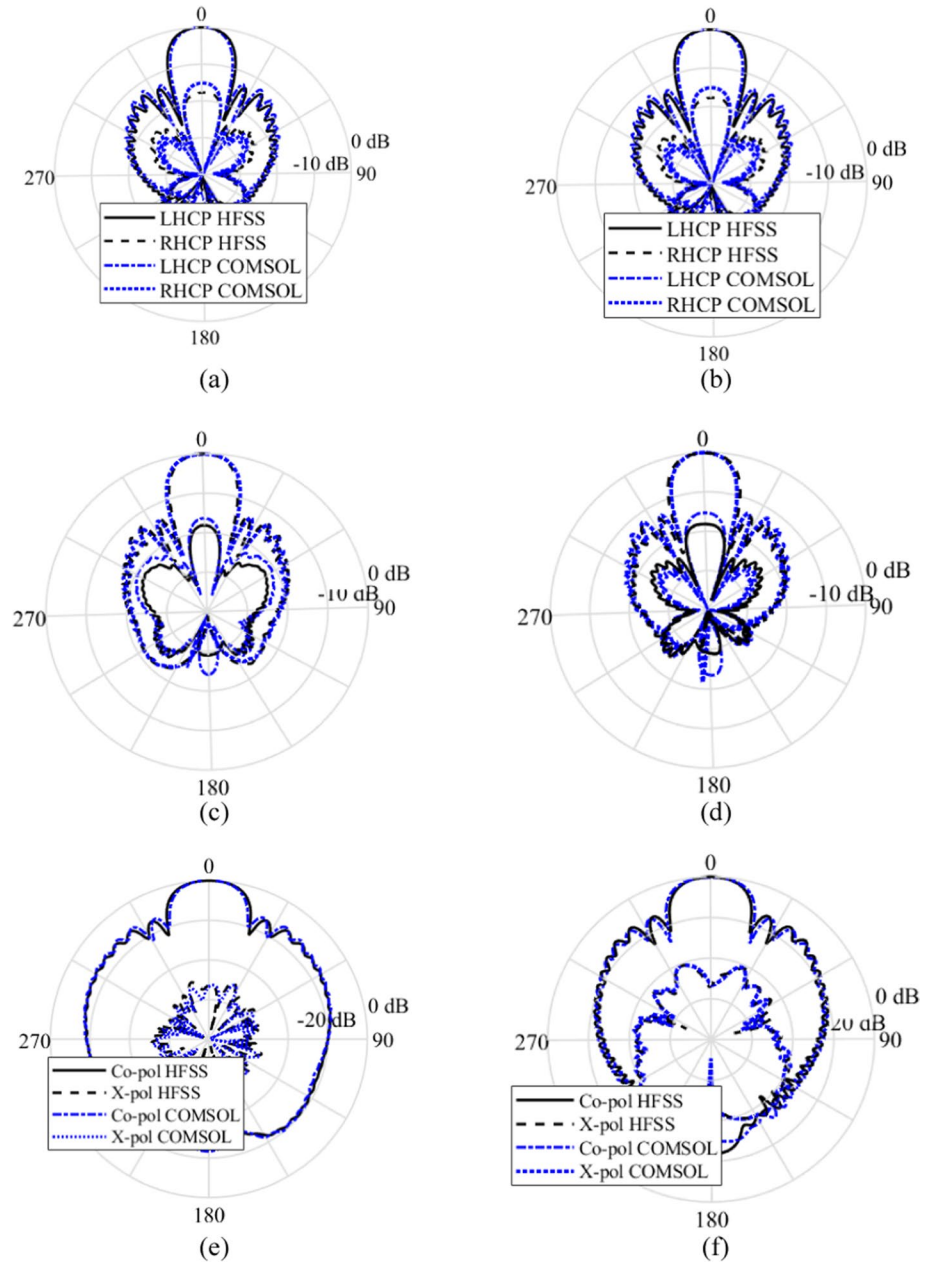
Fig. 6 The simulated radiation patterns of the proposed THz antenna, **a** $B_0 = -4.6Ta_z$ at 3 THz in XoZ plane, **b** $B_0 = -4.6Ta_z$ at 3 THz in YoZ plane, **c** $B_0 = 4.6Ta_z$ at 3THz in XoZ plane, **d** $B_0 = 4.6Ta_z$ at 3THz in YoZ plane, **e** $B_0 = 0Ta_z$ at 3.3 THz in XoZ plane, and **f** $B_0 = 0Ta_z$ at 3.3 THz in YoZ plane. Other parameters of graphene are: $\mu_c = 0.23eV, T = 300K, \tau = 0.9ps$

Fig. 7 The comparison between the simulation results with two different solvers **a** reflection coefficients, **b** axial ratios, and **c** gains. Other parameters of graphene are $\mu_c = 0.23eV, T = 300K, \tau = 0.9ps$, $B_0 = +4.6a_z$

(a)

(b)

(c)
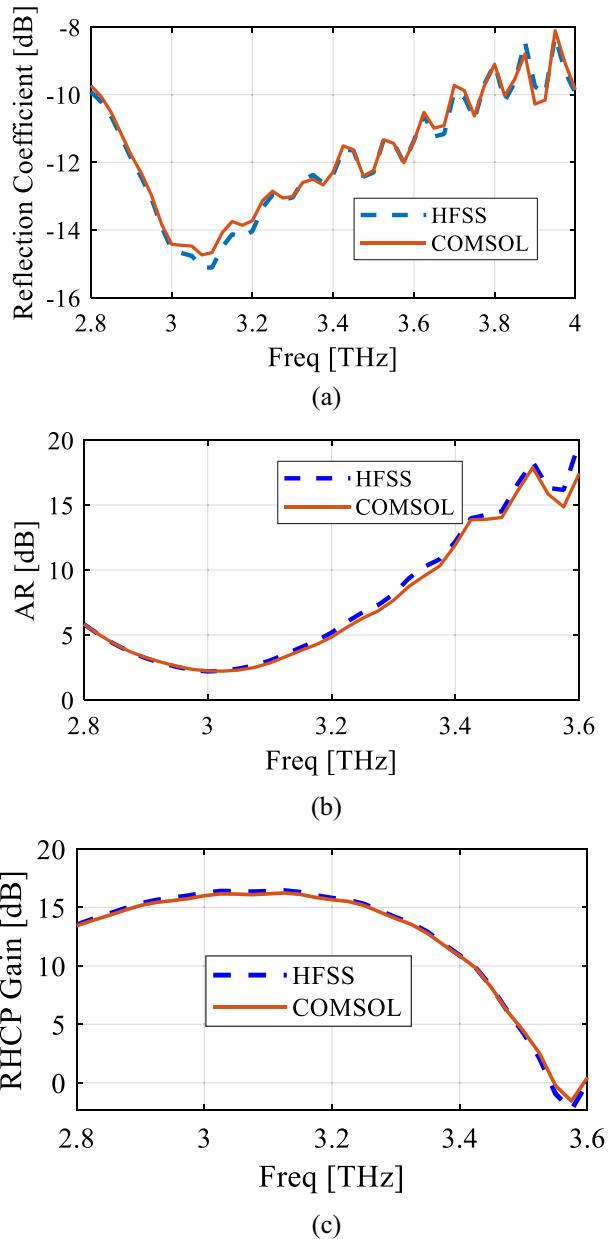
5 Conclusion

This article discusses the use of magnetically biased graphene to create a terahertz antenna that can change the polarization of the radiation pattern. The antenna allows terahertz waves to enter through a slot aperture from a microstrip transmission line. These waves are then coupled to a silicon dielectric resonator, which has a graphene

Table 2 Comparison between the proposed polarization reconfigurable THz antenna and the other works reported in the literature

References	Structure	$f_0[THz]$	Polari-zation control parameter	Efficiency (%)
Zhang et al. (2021b)	Antenna Based on Graphene Meta-surface	1, 2.5	μ_c	-
Kiani et al. (2021a)	Four-Leaf Clover-Shaped	0.65	μ_c	LP:25 CP: 14
Kiani et al. (2021b)	Graphene-loaded microstrip antenna	0.65	μ_c	LP:62 CP: 21
Kiani et al. (2022)	Graphene-loaded microstrip antenna	0.59	μ_c	LP:50 CP: 16.2
Kiani et al. (2020)	Graphene-loaded microstrip antenna	0.67	μ_c	LP:41 CP: 25
Kiani et al. 2021c)	Graphene-loaded microstrip antenna	0.75	μ_c	LP:51 CP: 45
Chashmi et al. (2019)	Y-shaped graphene-based antenna	0.95	μ_c	27
Chashmi et al. (2020a)	Y-shaped graphene-based antenna	0.44	μ_c	> 24
Chashmi et al. (2020b)	Graphene loaded microstrip antenna	0.8–1.07 0.975–1.025	μ_c	16–40
Kiani et al. (2023c)	graphene-based THz patch antenna	1.25	μ_c	59
This work	Proposed dielectric rod antenna	3	Magnetic flux density B_0	LP:85 CP:70

layer on top. This setup enables the launch of terahertz surface waves within the silicon dielectric rod. By applying a magnetic field perpendicular to the antenna, the graphene's conductivity tensor exhibits non-diagonal elements, resulting in circular polarization. The authors employ the Modified Relaxation-Effect model to calculate the losses of silver metal at terahertz frequencies. This model is more accurate than the skin effect model used for microwave frequencies. The results show remarkable impedance matching for linear and circular polarizations in the 2.86 to 3.14 THz range.

Declarations

Ethics approval and consent to participate Not applicable.

Consent for publication The Author hereby consents to publication of the Work in Infrared, Millimeter, and Terahertz Waves journal.

Conflict of interest Not applicable.

References

Ahmadi, E., Fakhte, S., Hosseini, S.S.: Dielectric rod nanoantenna fed by a planar plasmonic waveguide. Opt. Quantum Electron. **55**(2), 115 (2023)

Ali, Q., Shahzad, W., Ahmad, I., Safiq, S., Bin, X., Abbas, S.M., Sun, H.: Recent developments and challenges on beam steering characteristics of reconfigurable transmitarray antennas. Electronics **11**(4), 587 (2022)

Ali, M., Rivera, A., García-Muñoz, L.E., Gallego, D., Lyubchenko, D., Xenidis, N., Carpintero, G.: Dielectric rod waveguide-based radio-frequency interconnect operating from 55 GHz to 340 GHz. In: 2022 47th International Conference on Infrared, Millimeter and Terahertz Waves (IRMMW-THz), pp. 1–2. IEEE (2022)

Ali, M., Tebart, J., Rivera-Lavado, A., Lioubtchenko, D., Garcia-Muñoz, L.E., Stöhr, A., Carpintero, G.: Terahertz band data communications using dielectric rod waveguide. In: Optical Fiber Communication Conference, pp. W1H-5. Optica Publishing Group (2022)

Aqlan, B., Himdi, M., Vettikalladi, H., Le-Coq, L.: A circularly polarized sub-terahertz antenna with low-profile and high-gain for 6G wireless communication systems. IEEE Access **9**, 122607–122617 (2021)

Chashmi, M.J., Rezaei, P., Kiani, N.: Reconfigurable graphene-based V-shaped dipole antenna: from quasi-isotropic to directional radiation pattern. Optik **184**, 421–427 (2019)

Chashmi, M.J., Rezaei, P., Kiani, N.: Y-shaped graphene-based antenna with switchable circular polarization. Optik **200**(2020), 163321 (2020a)

Chashmi, M.J., Rezaei, P., Kiani, N.: Polarization controlling of multi resonant graphene-based microstrip antenna. Plasmonics **15**, 417–426 (2020b)

Dolatabady, A., Granpayeh, N.: Manipulation of the Faraday rotation by graphene metasurfaces. J. Magn. Magn. Mater.magn. Magn. Mater. **469**, 231–235 (2019)

Dukhopelnykov, S.V., Lucido, M., Sauleau, R., Nosich, A.I.: Circular dielectric rod with conformal strip of graphene as tunable terahertz antenna: interplay of inverse electromagnetic jet, whispering gallery and plasmon effects. IEEE J. Sel. Top. Quantum Electron. **27**(1), 1–8 (2020)

Elayan, H., Amin, O., Shubair, R.M., Alouini, M.-S.: Terahertz communication: the opportunities of wireless technology beyond 5G. In: 2018 International Conference on Advanced Communication Technologies and Networking (CommNet), pp. 1–5. IEEE (2018)

Johnk, C.T.A.: Engineering electromagnetic fields and waves. New York (1975)

Fakhte, S., Taskhiri, M.M.: Polarization-reconfigurable terahertz dielectric resonator antenna utilizing the magneto-optical characteristics of graphene. Under Review (2023)

Fakhte, S., Taskhiri, M.M.: Dual-band terahertz dielectric resonator antenna with graphene loading. Optic Quantum Electron **54**(12), 845 (2022)

Gusynin, V., Sharapov, S., Carbotte, J.: Magneto-optical conductivity in graphene. J. Phys. Condens. Mattercondens. Matter **19**, 026222 (2006)

He, Y., Chen, Y., Zhang, L., Wong, S.-W., Chen, Z.N.: An overview of terahertz antennas. China Commun. **17**(7), 124–165 (2020)

Huang, J., Chen, S.J., Xue, Z., Withayachumnankul, W., Fumeaux, C.: "Wideband circularly polarized 3-D printed dielectric rod antenna. IEEE Trans. Antennas Propag. **68**(2), 745–753 (2019)

Khan, M.S., Jahnavi Priya, B., Aishika, R., Varshney, G.: Implementing the circularly polarized THz antenna with tunable filtering characteristics. Results Opt **11**, 100377 (2023)

Kiani, N., Hamedani, F.T., Rezaei, P., Chashmi, M.J., Danaie, M.: Polarization controling approach in reconfigurable microstrip graphene-based antenna. Optik **203**, 163942 (2020)

Kiani, N., Hamedani, F.T., Rezaei, P.: Polarization controlling method in reconfigurable graphene-based patch four-leaf clover-shaped antenna. Optik **231**, 166454 (2021a)

Kiani, N., Hamedani, F.T., Rezaei, P.: Polarization controlling plan in graphene-based reconfigurable microstrip patch antenna. Optik **244**, 167595 (2021b)

Kiani, N., Hamedani, F.T., Rezaei, P.: "Polarization controlling idea in graphene-based patch antenna. Optik **239**, 166795 (2021c)

Kiani, N., Hamedani, F.T., Rezaei, P.: Realization of polarization adjusting in reconfigurable graphene-based microstrip antenna by adding leaf-shaped patch. Micro Nanostruct. **168**, 207322 (2022)

Kiani, N., Hamedani, F.T., Rezaei, P.: Designing of a circularly polarized reconfigurable graphene-based THz patch antenna with cross-shaped slot. Opt. Quantum Electron. **55**(4), 356 (2023a)

Kiani, N., Hamedani, F.T., Rezaei, P.: Reconfigurable graphene-gold-based microstrip patch antenna: RHCP to LHCP. Micro Nanostruct. **175**, 207509 (2023b)

Kiani, N., Hamedani, F.T., Rezaei, P.: Designing of a circularly polarized reconfigurable graphene-based THz patch antenna with cross-shaped slot. Opt. Quant. Electron. **55**, 356 (2023c). https://doi.org/10.1007/s11082-023-04617-y

Larki, F., Kameli, P., Nikmanesh, H., Jafari, M., Salamati, H.: The influence of external magnetic field on the pulsed laser deposition growth of graphene on nickel substrate at room temperature. Diam. Relat. Mater. Relat. Mater. **93**, 233–240 (2019)

Liu, X., Schmitt, L., Sievert, B., Lipka, J., Geng, C., Kolpatzeck, K., Erni, D., et al.: Terahertz beam steering using a MEMS-based reflectarray configured by a genetic algorithm. IEEE Access **10**, 84458–84472 (2022)

Lucyszyn, S.: Evaluating surface impedance models for terahertz frequencies at room temperature. Piers **3**(4), 554–559 (2007)

Luo, Y., Zeng, Q., Yan, X., Yong, Wu., Qichao, Lu., Zheng, C., Nan, Hu., Xie, W., Zhang, X.: Graphene-based multi-beam reconfigurable THz antennas. IEEE Access **7**, 30802–30808 (2019)

Lv, X.-L., Bian, Wu., Zhao, Y.-T., Hao-Ran, Zu., Wei-Bing, Lu.: Dual-band dual-polarization reconfigurable THz antenna based on graphene. Appl. Phys. Express **13**(7), 075007 (2020)

Moradi, K., Karimi, P.: An enhanced gain of frequency and polarization reconfigurable graphene antenna in terahertz regime. AEU-Int. J. Electron. Commun. **158**, 154463 (2023)

Nasir, M., Xia, Y., Jiang, M., Zhu, Qi.: A novel integrated Yagi-Uda and dielectric rod antenna with low sidelobe level. IEEE Trans. Antennas Propag. Propag. **67**(4), 2751–2756 (2019)

Nasir, M., Xia, Y., Sharif, A.B., Guo, G., Zhu, Q., Ur Rehman, M., Abbasi, Q.H.: A high gain embedded helix and dielectric rod antenna with low side lobe levels for IoT applications. Sensors **22**(20), 7760 (2022)

Pawar, A.Y., Sonawane, D.D., Erande, K.B., Derle, D.V.: Terahertz technology and its applications. Drug Invent. Today **5**(2), 157–163 (2013)

Petrov, V., Pyattaev, A., Moltchanov, D., Koucheryavy, Y.: Terahertz band communications: Applications, research challenges, and standardization activities. In: 2016 8th International Congress on Ultra modern Telecommunications and Control Systems and Workshops (ICUMT), pp. 183–190. IEEE (2016)

Rasilainen, K., Phan, T.D., Berg, M., Pärssinen, A., Soh, P.J.: Hardware aspects of sub-THz antennas and reconfigurable intelligent surfaces for 6G applications. IEEE J. Sel. Areas Commun. (2023)

Rivera-Lavado, A., García-Muñoz, L.-E., Lioubtchenko, D., Preu, S., Abdalmalak, K.A., Santamaría-Botello, G., Segovia-Vargas, D., Räisänen, A.V.: "Planar lens–based ultra-wideband dielectric rod waveguide antenna for tunable THz and sub-THz photomixer sources. J. Infrared, Millimeter Terahertz Waves **40**, 838–855 (2019)

Shiau, Y.: Dielectric rod antennas for millimeter-wave integrated circuits. IEEE Trans. Microw. Theory Techn. **MTT-24**(11), 869–872 (1976)

Singhwal, S.S., Matekovits, L., Kanaujia, B.K., Kishor, J., Fakhte, S., Kumar, A.: Dielectric resonator antennas: applications and developments in multiple-input, multiple-output technology. IEEE Antennas Propag. Mag. Propag. Mag. **64**(3), 26–39 (2022). https://doi.org/10.1109/MAP.2021.3089981

Song, H.-J., Nagatsuma, T.: Present and future of terahertz communications. IEEE Trans. Terahertz Sci. Technol. **1**(1), 256–263 (2011)

Sounas, D.L., Caloz, C.: Gyrotropy and nonreciprocity of graphene for microwave applications. IEEE Trans. Microw. Theory Tech. Microw. Theory Tech. **60**(4), 901–914 (2012)

Sugimoto, Y., Sakakibara, K., Kikuma, N.: Narrow-pitch angle multibeam dielectric lens antenna illuminated by dielectric rod antennas. In: 2022 IEEE International Symposium on Antennas and Propagation and USNC-URSI Radio Science Meeting (AP-S/URSI), pp. 543–544. IEEE (2022)

Tamagnone, M., Slipchenko, T.M., Moldovan, C., Liu, P.Q., Centeno, A., Hasani, H., Zurutuza, A., et al.: "Magnetoplasmonic enhancement of Faraday rotation in patterned graphene metasurfaces. Phys. Rev. B **97**(24), 241410 (2018)

TDK Corporation, "B66335G2000X127 : Detailed information | ferrites and accessories - ferrite cores," TDK Product Center, 2023. https://product.tdk.com/en/search/ferrite/ferrite/ferrite-core/info?part_no=B66335G2000X127 (Accessed Sep. 27, 2023).

Varshney, G., Debnath, S., Sharma, A.K.: "Tunable circularly polarized graphene antenna for THz applications. Optik **223**, 165412 (2020)

Venkatesh, S., Xuyang, Lu., Saeidi, H., Sengupta, K.: A programmable terahertz metasurface with circuit-coupled meta-elements in silicon chips: creating low-cost, large-scale, reconfigurable terahertz metasurfaces. IEEE Antennas Propag. Mag.propag. Mag. **64**(4), 110–122 (2022)

Wu, G.B., Zeng, Y.-S., Chan, K.F., Qu, S.-W., Chan, C.H.: High-gain circularly polarized lens antenna for terahertz applications. IEEE Antennas Wirel. Propag. Lett. **18**(5), 921–925 (2019)

Yang, G., Zhang, N., Song, R., Cui, G., Liu, N., Liu, J.: Terahertz windmill-shaped circularly polarized pattern reconfigurable antenna with MEMS switches. In: 2022 IEEE 9th International Symposium on Microwave, Antenna, Propagation and EMC Technologies for Wireless Communications (MAPE), pp. i-v. IEEE (2022)

Zhang, J., Tao, S., Yan, X., Zhang, X., Guo, J., Wen, Z.: Dual-frequency polarized reconfigurable terahertz antenna based on graphene metasurface and TOPAS. Micromachines **12**(9), 1088 (2021a)

Zhang, J., Tao, S., Yan, X., Zhang, X., Guo, J., Wen, Z.: Dual-frequency polarized reconfigurable terahertz antenna based on graphene metasurface and TOPAS. Micromachines **12**(9), 1088 (2021b). https://doi.org/10.3390/mi12091088